Synthesis, structure and theoretical simulation of a zinc(II) coordination complex with 2,3-pyridinedicarboxylate

Sarra Soudani, Melek Hajji, Jin Xiao X Mi, Christian Jelsch, Fréderic Lefebvre, Taha Guerfel, Cherif Ben Nasr

Published in *Journal of Molecular Structure*, **2020**. *1199*, 127015.

doi.org/10.1016/j.molstruc.2019.127015

Synthesis, structure and theoretical simulation of a zinc(II) coordination complex with 2,3-pyridinedicarboxylate

Sarra Soudani [1] • Melek Hajji [2]• Jin Xiao Mi [3] • Christian Jelsch [4] • Frederic Lefebvre [5] • Taha Guerfel [2] • Cherif Ben Nasr [1, ¥]

[1] Laboratoire de Chimie des Matériaux, Faculté des Sciences de Bizerte, Université de Carthage, 7021 Zarzouna, Tunisia.

[2] Research Unit: Electrochemistry, Materials and Environment, University of Kairouan, 3100 Kairouan, Tunisia.

[3] Dept. of Materials Science and Engineering, College of Materials, Xiamen University, Xiamen 361005, Fujian Province, People's Republic of China

[4] CRM^2, CNRS, Institut Jean Barriol, Université de Lorraine, Vandoeuvre les Nancy CEDEX, France.

[5] Laboratoire de Chimie Organométallique de Surface (LCOMS), Ecole Supérieure de Chimie Physique Electronique, 69626 Villeurbanne Cedex, France.

[¥] Correspondence e-mail: cherif.bennasr@fsb.rnu.tn

Abstract

Hydrolytic opening reaction of 2,3-pyridine dicarboxylic anhydride with the zinc dichloride led to form the chelate complex of mono deprotonated 2,3-pyridine dicarboxylic acid, $[Zn(2,3\text{-pdcH})_2(H_2O)_2]$, (2,3-pdcH = 2,3-pyridinedicarboxylic acid). The coordinated compound crystallizes in the monoclinic space group $P2_1/n$. The crystal structure of the title compound exhibits a homoleptic complex with distorted octahedral geometry and ligand coordinated via pyridine nitrogen and oxygen atoms from one deprotonated dicarboxylic acid. Intermolecular interactions were analysed by Hirshfeld surfaces. After formation of the metal complex, the crystal packing is stabilized by O-H…O and C-H…O hydrogen bonds. There are moreover hydrophobic interactions, which consist in stacking between the pyridine cycle and the carboxylic/carboxylate groups. NBO and QTAIM analyses have been performed to evaluate the charge delocalization interactions that occur between the Zn(II) central ion and the surrounding ligand donor atoms. The HOMO and LUMO energies and Molecular Electrostatic Potential surface were derived from DFT theoretical calculations.

Keywords Zn(II) chelate complex • Hirshfeld surface • Metal-Ligand interaction • 2,3-pyridinedicarboxylate ligand • DFT

1. Introduction

In the recent years, many researchers have been interested to synthesize coordination compounds due to their versatile applications and its wide chemical properties. Moreover, the coordination of ligands with various metal transition allowed to form a variety of supramolecular architectures with an extensive network of hydrogen bonding [1] and coordination polyhedra such as tetrahedral, square planar, square pyramidal, trigonal bipyramidal and octahedral [2-4]. As is well known, the structural diversity of ligands and the choice of metals are the most important aspects of coordination chemistry. Among ligands, salts of the carboxylate groups and aromatic pyridines rings describe attractive multifunctional building blocks in the formation of coordination complexes and exhibit interesting molecular structures [5]. Additionally, Metal coordinated compounds based on carboxylate ligands play a very great role in material chemistry, such as catalysis [6,7], medicinal chemistry [8], photochemistry and electrochemistry [9] and so on. In this context, the 2,3-pyridine dicarboxylic anhydride is commonly used as a linker to construct coordination compounds which can adopt varied coordination modes such as monodentate, chelating bidentate, bridging bidentate and multidentate. This could potentially allow different coordination motifs to form infinite molecular structures with various metal centers. The carboxylic O atoms are favourable to form hydrogen bonding, while the pyridyl ring is usually able to form of stacking interactions. The various coordination patterns of N or O atoms can result in novel structures and topologies [10]. The hydrolysis reaction of the 2,3-pyridine dicarboxylic anhydride can open the ring of the carboxylic anhydride either to give a dicarboxylic acid or to prepare different carboxylate complexes [11] presenting strong and weak intermolecular interactions which give stability and H-bonded supramolecular network in the crystal packing.

In our continuation of synthesis and structural studies of carboxylate complexes, it was of great research interest to study the synthesis, structural characterization and theoretical simulation of a zinc(II) complex based on 2,3 pyridine dicarboxylic acid.

2. Experimental

2.1. Chemical preparation

All chemical and solvents used in this work were purchased by Sigma-Aldrich and used as received with the purity available.

A solution of $ZnCl_2$ ((0.137 g, 1 mmol) dissolved in water (6 mL) was added dropwise to a solution of 2,3-pyridine dicarboxylic anhydride (0.3 g, 2 mmol) in water. After stirring for

one hour, the resultant solution was evaporated at room temperature. The transparent crystals of the compound were isolated after few days and subjected to X-ray diffraction analysis (yield 86%). Anal. Calc.: C, 38.34 %; H, 2.76 %; N, 6.45 %. Found: C, 37.99 %; H, 2.63 %; N, 6.89 %.

The same compound is also synthesized by Aghabozorg *et al.,* which obtained it with an aqueous solution of 2,9-dimethyl-1,10-phenathroline, pyridine-2,3-dicarboxylic and the $ZnSO_4.7H_2O$ [12].

2.2. Investigation techniques

2.2.1. X-ray single crystal structural analysis

The single-crystal X-ray diffraction experiment was carried out using a Bruker Apex CCD diffractometer equipped with Mo radiation source (λ=0.71073Å). Intensities were collected at 193 K by means of the *SMART* software [13]. Reflection indexing, unit-cell parameters refinement, Lorentz-polarization correction, peak integration and background determination were performed using the *SAINT* software [14]. The crystal structure was solved by direct methods and refined with the SHELXS 2013 [15]. The crystal data are gathered in Table 1. The drawings were made with Vesta [16] and Mercury [17]. Basic parameters describing the measurement procedure as well as the refinement results are shown in Table 1.

2.2.2. Multipolar calculations

The charge density of the molecules was modelled using the Hansen & Coppens multipolar atom [18]. The charge density parameters were transferred from the ELMAM2 database of multipolar atoms [19]. The X-H bond lengths were elongated according to standard neutron diffraction distances [20]. The electrostatic energy was computed with the VMoPro module of MoPro software [21] between pairs of atoms in close contact. The energy was obtained by direct summation over contacts between the reference and the surrounding molecules. To take into account only the shortest contacts which contribute to the Hirshfeld surface contacts atom/atom decomposition, a cut-off of the sum of van der Waals radii plus 0.2 Å was applied to the interatomic distance. Average E_{elec} values were obtained by dividing the summation by the number of contacts. Hirshfeld surface and contact enrichment ratios were obtained with MoProViewer [22]. As X…Y and Y…X contact types yield similar contact surfaces and E_{elec} values in the context of this study, the reciprocal contacts were merged together.

2.2.3. Computational methodologies and software

All DFT computations were carried out starting from the experimental X-ray structure as input geometry. The Becke's three parameter hybrid exchange and nonlocal correlation functional of Lee, Yang and Parr (UB3LYP) [23-25] were used. A quasi-relativistic Stuttgart/Dresden (SDD) effective core potential [26] was applied on Zn, and 3-21 basis set on all other elements. Frequency calculations indicate that all stationary points were found to be true minima (zero imaginary frequency) on the potential energy surface. For Natural Bond Orbital (NBO), Quantum Theory of Atoms-in-Molecules (QTAIM) and Frontier Molecular Orbitals (FMO) analysis… more accurate energies were obtained by performing single point calculations using larger standard basis set 6-31+G*/SDD, starting from optimized structures. Gaussian 09, Rev D.01 software package [27] was employed for all calculations. GaussView 6.0 program [28] and AVOGADRO 1.2.0 molecular viewer [29] were used to visualize, analyze, modify and export results.

3. Results and discussion

3.1. Structure description

Crystallographic data, refinement results and intensity data of the coordinated compound are presented in Table 1. The bond lengths and angles are given in Table 2 whereas hydrogen bonds present in the crystal structure are shown in Table 3. The reaction of 2,3-pyridine dicarboxylic anhydride with zinc dichloride in water gives rise to a chelate complex with the formula $[Zn(2,3\text{-pdcH})_2(H_2O)_2]$ (Fig. 1). There is also a report of a similar zinc compound with pyridine-2,3-dicarboxylic acid [12]. In this complex structure, each ligand coordinates in a chelate mode via both nitrogen and oxygen atoms from a deprotonated 2-carboxylic acid group, forming a five-membered chelate ring. The remaining protonated carboxylic group is involved in the formation of intramolecular hydrogen bonds, O4-H4…O3 ($d_{D–A}$ = 2.399 Å and D–H---A 174°) and not in coordination. The Zn atom is hexacoordinated to two oxygen atoms (O1, $O1^i$ (*i*= 1-*x*, 1-*y*, 1-z)) of two water molecules, to two oxygen atoms (O2, $O2^i$) and two nitrogen atoms (N1, $N1^i$) of the 2,3—pdcH ligand. The atoms O2, $O2^i$, N1 and $N1^i$ occupy the equatorial positions, while the atoms O1 and $O1^i$ are located on the axial positions occupying trans-positions. The geometrical features of the ZnO_4N_2 octahedron are reported in Table 2. The N- Zn-O angles range from 78.45(6) ° to 101.55(6) °. The three angles around the Zn atom (O1-Zn-$O1^i$, O2-Zn-$O2^i$ and N1-Zn-$N1^i$ are all flat with angles value equal to 180°, giving octahedral geometry (Fig. 2 & 3). The detailed geometry of the ZnO_4N_2 octahedra (Table 2) shows that the bond distances (Zn1-N1 = 2.0645(15) Å, Zn1-O2 = 2.0551(13) Å and Zn-O1= 2.1874(15) Å compare well to those reported for similar octahedral

Zn(II) complexes [11]. The bond angles around the Zn atom vary between 78.45(6) and 101.55(6)° indicating that the ZnN_2O_4 species have a slightly distorted octahedral geometry. It is worth to note that in the lattice structure, the [Zn(2,3-pdcH)$_2$(H_2O)$_2$] entities are situated on the vertices and the middle of the unit cell (Fig. 2). The dihedral angle between the plane containing the water molecules and that of the pyridine dicarboxylic acid is 87.96° (Fig. 3) underlining non-orthogonal arrangement between these groups. The structure of organic cation contains an unusual COOH carboxylic acid with the proton lying in the anti-position [30]. This is due to a stabilization of the anti-conformation by an intramolecular hydrogen bond. The great abundance of hydrogen bonding donors and acceptors gives origin to a complex three-dimensional hydrogen bonding network. The carboxylate group shows strong intramolecular hydrogen bonding (O4—OH4···O3) between the OH group of the neutral carboxylic acid and the carbonyl oxygen of another coordinating carboxylate group. Each [Zn(2,3-pdcH)$_2$(H_2O)$_2$] entity is connected via the formation of O-H…O (O1—OW1···O5 and O1—OW2···O5 (symmetry codes: $-x+½, y-½, -z+^3/_2$ and $x+1,y,z$ respectively) hydrogen bonds involving both coordinated water molecules to four neighboring [Zn(2,3-pdcH)$_2$(H_2O)$_2$] entities (Fig.4). These moieties are connected via C-H…O (C2—H2···O2 and C2—H2···O3) hydrogen bonds to form layers parallel to the (**a**,**b**) plane (Fig. 5).

3.2. Metal—ligand charge-transfer interaction (MLCTI) analysis

Natural Population Analysis (NPA) and Natural Bond Orbital (NBO) were primarily investigated to predict the molecular natural charge distribution and also to exhaustively explore the strength and nature of the charge delocalization interactions that occur between the ligand and the zinc metal atoms. The NPA-NBO framework is the most suitable approach for atomic charge computations, since it is less affected by basis set changing. The existence of both nitrogen and oxygen as ligand coordinated atoms offers an occasion to enrich the inquiry of electron donation tendency. The natural atomic charges and valence electron configurations on the atoms of the coordinated ligands as well as the Zn metal ion are summarized in Table 4, on account of the symmetry half of the data are presented. Interestingly, the net natural charge at the Zn cation is 1.05956 e. This value is considerably lower than the formal charge (+2) suggesting that charge of zinc cation was meaningfully diminished by the negative electron density transferred from the ligand units. The net charges at O1, O2 and N1 ligand atoms are -0.75829, -0.68286 and -0.52609 e, respectively. These results indicate the transfer of a significant amount of electron density to the zinc atom by 0,24171, 0,31714 and 0,47391 e from O1, O2 and N1 nitrogen atom, respectively. It is clearly

shown that the water molecule, which has O1 as interacted atom, has a slighter ability towards electron donation to the Zn^{2+}cation. Remarkably, the central zinc atom has an d^{10} valence configuration, however investigating the orbital populations we find the following valence arrangement [$4S^{0.37}3d^{9.99}4p^{0.56}5p^{0.02}$]. Additionally, from Table 4, all coordination ligand atoms have a valence electron configuration lower than these expected. Therefore, the studied complex could be described as a ligand-to-metal charge-transfer (LMCT) complex since the donations from ligand to metal are higher than the back donation. The Zn—O and Zn—N interactions were carefully discussed through NBO—Second-order perturbation theory. The second order perturbative energies $E^{(2)}$ corresponding to donor-acceptor interactions between ligand donor orbitals (NBO(i)) and metal acceptor orbitals (NBO(j)) are reported in Table 5. The hybridizations, occupancies and energies of these orbitals are given in Table 6. At first sight, we notice that the studied system does not incorporate a bond BD (electron pairs centered on two atoms) between interacted O/N atoms and Zn^{2+} cations, seeing that the Zn—O/N interactions are coming from an electronic delocalization between the O/N-lone pair filled orbitals LP(O/N) to the empty anti-bonding orbitals of the Zn metal LP*(Zn). As shown in Figures 6 and 7, all LP donor NBOs present a mixed s/p character, except for LP(3)O2 which is a p pure orbital. On the other hand, all LP* metal acceptor NBOs are pure p orbitals excepting LP*(6)Zn which shows a nearly s character (Table 6). The net stabilization energies (given in bold in Table 5) for Zn—O1, Zn—O2 and Zn—N1 are 87.22, 144.12 and 98.44 kcal/mol, respectively. These results are consistent with the reported X-ray bond distances as shorter bond length favors a higher electronic delocalization [31]. As a result of the charge transfer process, considerable shifts in the occupancies of interacted orbitals as well as their energies happened (Table 6). Although the LP(3)O2 NBO has lower energy (-0.32133) and lesser occupancy (1.61113) with respect to other donor orbitals, it is not responsible for the greatest interactions with the Zn anti-bonding NBOs. In fact, as clearly shown in Fig. 7, this orbital is engaged in another strong interaction LP(3)O2→BD*(2)C6-O3 as an electron withdrawing center with associated $E^{(2)}$ value of 165.22 kcal/mol. This explains why this NBO atom loses more electrons. Furthermore, it is noticed from data collected in Tables 5 and 6, that it is not evident that donor orbitals with higher levels of energy have higher $E^{(2)}$ values. This is in agreement with previous conclusions on the subject [32]. Moreover, we found from the NBO analysis that electronic delocalizations from LP(Zn) and LP*(Zn) to some RY* of the oxygen and nitrogen atoms occur although with lower energies, where RY* designates the 1-center Rydberg non-Lewis NBOs. Based on Bader's quantum theory of atoms-in-molecules (QTAIM) tool, the donor-acceptor connection between the metal and the surrounding ligands

was further discussed. Topological properties at the Zn—N and Zn—O bond critical points (BCPs) are given in Table 7. QTAIM-molecular graph for complex **1** is illustrated in Figure 8. The estimated electron density and its Laplacian values $(\rho; \nabla^2\rho)$ at bond critical point are equal to (0.03334; 0.20592) , (0.04687; 0.37657 u.a) and (0.05415; 0.42090) for Zn—O1, Zn—O2 and Zn—N1, respectively. Generally, all these amounts are coherent with shared (covalent or similar) bonds [33]. Additionally, for all bonds, the total energy density H_c is negative and the $|V_c|/G_c$ ratio is > 1 indicating the predominant covalent character [34]. The interaction energies at the BCPs were determined from the electron potential energy density as $E_{int} = V(r)/2$ and found to be -21.77, -29.78 and -29.54 for Zn—O1, Zn—O2 and Zn—N1, respectively. These values are qualitatively correlated to bond lengths with the fact that the shorter the atom–atom distances, the greater the orbital overlaps, as already reported for similar systems [35-37].

3.3. Hirshfeld surface and enrichment ratio

Studies of intermolecular interactions using the Hirshfeld surface represents an important tool to gain insight into crystal structure. The Hirshfeld surface was computed with the MoProViewer software [22]. The enrichment ratios [38] of contacts between the different chemical species were computed in order to highlight which contacts are statistically over-represented and favored in the crystal packing. The chemical nature of contacts and their enrichment ratios in the title compound are shown in Table 8 and Fig. 9. A dimer of the asymmetric unit was generated as the Zn(II) cation lies on an inversion center with multiplicity 2. To obtain an integral Hirshfeld surface around each entity (water, Zn^{++}, organic anion), a set of entities not in contact with each other were selected in the crystal packing (Fig. 9 and Fig. 10). The Hirshfeld surface of the ensemble is constituted by as much as 31% of oxygen atoms followed by carbon at 25.5%. and the water Ho and hydrophobic Hc hydrogen atom types. The major contacts are constituted by strong O-H…O and weak C-H…O hydrogen bonds followed by C…O contacts and Zn…O coordination. The C…O interactions can be quite favorable from an electrostatic point of view as within the COOH and COO^- moieties, the carbon $C^{\delta+}$ and oxygen $O^{\delta-}$ atoms bear charges of opposite sign. There is a significant parallel stacking between the COOH and COO^- planar groups. The Zn(II) cation is coordinated by the unique nitrogen atom resulting in a high enrichment ratio E_{ZnN}=7.11. The metallic cation is also coordinated by two oxygen atoms (on the carboxylic acid and on the water molecule, E_{ZnO}=1.77). The non-polar species, C and Hc, have quite enriched self-contacts which are related to the extensive stacking occurring between organic

flat molecules. The planes of the organic cation show two orientations, related by a 2-fold helicoidal axis along **b**, forming an angle of 37.9°. Due to these two close orientations of organic cations, there are no C-H… π weak hydrogen bonds (where the C-H direction is not far from being perpendicular to the sp^2 plane). Besides the hydrophobic contacts, Hc atoms form weak C-H…O hydrogen bonds which are significantly over-represented at E_{OHc}=1.61. The polar water Ho hydrogen atoms are mostly in contacts with oxygen atoms, notably a strong O-H…O hydrogen bond with the C=O group of the carboxylic acid. O…Ho contacts are slightly more enriched (E=1.82) than O…Hc. The self-contacts between charged species (Zn^{++}, $N^{\delta-}$, $O^{\delta-}$ and $Ho^{\delta+}$) have E_{xx} values very close to zero and are systematically avoided, due to electrostatic repulsion. This can be seen in Fig. 11 which shows the relationship between enrichment ratios E_{xy} and average electrostatic energy E_{elec} of the different contact types. Globally, there is a clear correlation between $<E_{elec}>$ and E_{xy} values. The two strong negative electrostatic energies correspond to most enriched contacts: Zn…N followed by Zn…O. The scatterplot in Fig. 11 suggests that the driving force in the crystal stabilization is the formation of the coordination complex followed by the strong O…Ho and the weak O…Hc hydrogen bonds.

Analyzing the Hirshfeld surface and contacts once the metal complex of Zn(II) with two anions and two water molecules is formed gives a different and more supramolecular picture of the crystal packing (**Table 9**). The surface content is then half hydrophilic and half hydrophobic. For the formed complex, the major surface contacts are strong O-H…O and weak C-H…O hydrogen bonds together with C…O contacts. All these contacts are enriched, especially the hydrogen bonds. The extensive flat organic anion stacking results in well represented Hc…Hc and C..C self-contacts. When the metal/anions complex is considered as a whole moiety, there is no clear partition between hydrophobic (made of Hc and C atoms) and electrostatic contacts, as both represent ~24% of the contact surface, while cross interactions between charged and hydrophobic atoms represent 52% on the surface. This is notably due to an excess of hydrogen bond acceptors (COO^-, COOH, HOH) compared to only two strong hydrogen bond donors (HOH); this unbalance promotes the formation of weak C-H…O hydrogen bonds.

3.4. Frontier Molecular Orbitals analysis

The energy of frontier orbitals HOMO and LUMO plays a significant role in describing the chemical reactivity descriptors and chemical behavior of the chemical compounds. The

highest occupied molecular orbital (HOMO) is mainly localized on the carboxylic groups of the [Zn(2,3-pdcH)$_2$(H$_2$O)$_2$], (2,3-pdcH = 2,3-pyridinedicarboxylic acid), while the lowest unoccupied molecular orbital (LUMO) is mainly located on the carbon atoms of the ring and of one of the carboxylic groups. The energy gap between the HOMO and LUMO energies has been calculated as 4.71 eV (**Fig. 12**). This large energy gap characterizes a high chemical hardness and kinetic stability of the coordination compound [39]. As a consequence, this compound is stable in standard conditions. The density of state (DOS) spectrum of the title compound was plotted applying the Gauss Sum software using information from the Gaussian output file and is shown in **Fig. 13**. It shows the number of available molecular orbitals including compositions and their contributions to the chemical bonding at different levels of energies. From the DOS plot, the red and green lines of the plot indicate the virtual and occupied orbitals, respectively, and also provide an understanding of the molecular orbitals character in a particular area. The DOS plot and its energy levels also corroborated the Frontier Molecular Orbitals analysis.

3.5. Molecular Electrostatic Potential (MEP)

The molecular electrostatic potential surface (MEP) is performed to study the molecular reactive behavior towards electrophilic and nucleophilic attack and determine sites of electrophile (electron-deficient positively charged species) and the nucleophile (an electron rich, negatively charged species). The negative regions of the MEP which represent high electron density appear in red and are referred to the electrophilic reactivity while the positive (blue) regions are referred to the nucleophilic reactivity. As can be seen from **Fig. 14**, the red region located around the Zn atom can be considered as the electrophilic reactivity center while the positive region is localized on the ligand which will be the reactive sites for nucleophilic attack. This explains why these sites are involved in intermolecular contacts stabilizing the crystal [40-44]. The MEP surface shows that the negative potential sites situated on Zn atom while the positive potential sites situated around the ligand.

4. Conclusions

In this research, a complex [Zn(2,3-pdcH)$_2$(H$_2$O)$_2$] was obtained using a zinc dichloride salt and 2,3-pyridinedicarboxylic acid as ligand. The coordinated complex crystallizes in the monoclinic space group P21/n. The 2,3-pyridinedicarboxylic ligand coordinates in a bidentate chelate mode via the pyridine nitrogen atom and oxygen atom of the mono deprotonated 2-carboxylic group. The strongest electrostatic interactions are also the most enriched contacts

and are constituted by the N-Zn and O-Zn coordination bonds followed by strong O…Ho and weak O…Hc hydrogen-bonds. There are stacking interactions between the pyridine cycle and the COOH/COO^- groups resulting in significant C…C and $C^{\delta+}$…$O^{\delta-}$ contacts. The NBO—second-order perturbation theory analysis indicates that a two-center bond between the Zn^{2+} cations and O/N atoms was not found, the Zn—N/O interactions are coming from an electronic delocalization between the N/O filled nonbonding orbitals to the anti-bonding LP*(Zn) metal NBOs. Based on the atoms in molecules (AIM) results, all Zn—N/O interactions have a predominant coordinate covalent character. The MEP map define the nucleophile and the electrophile sites that the negative potential sites are on Zn(II) cation as well as the positive potential sites are around the 2,3-pyridinedicarboxylic ligand . The HOMO-LUMO energy gap suggest a good stability of the title compound. Exploitation of these computational findings for design and synthesis of new Zn(II) coordination complexes is currently ongoing.

Supplementary data

Crystallographic information is available at the Cambridge Crystallographic Data Centre, CCDC No 635310. These data can be obtained free of charge via http://www.ccdc.cam.ac.uk/conts/retrieving.html, or from the CCDC, 12 Union Road, Cambridge, CB2 1EZ, UK: fax: (+44) 01223-336-033; e-mail: deposit@ccdc.cam.ac.

Compliance with ethical standards

Conflict of interest: The authors declare that they have no conflict of interest.

Ethical statement: All ethical guidelines have been adhered.

References

1. N.O. Gopal, K.V. Narasimhulu, C.S. Sunandana, J. Lakshmana Rao, EPR and optical absorption spectral studies of Cr^{3+} ions doped in nickel maleate tetrahydrate single crystals. Physica B. 348 **(2004)** 335-340.

2. C. Ruizperez, J. G. Platas, H. Lotter, L. Lezama, X. Solans, S. Dominguez, P. M. Zarza, M. J. Rocio, M. S. Palacios, P. Gili, Structutre and properties of Cu(II) Oxypropiophenone-Salicylhydrazide)(2,2'-bipyridyl) [Cu(ohp-shz) (bipy)] and Cu(II) (o-hydroxypropiophenone-salicylhydrazide) (2,2'-bipyridylamine) monohydrate [Cu(ohp-shz) (bipyam)H2O, Inorg Chim Acta 255 **(1997)** 139-148.

3. LH. Uppadine, J. P. Gisselbrecht, J. M. Lehn, Protonic modulation of redox properties in ionisable [2 2] grid-like metalloarrays, Chem. Commun 6 **(2004)** 718-719.

4. L. H. Uppadine, J. M. Lehn, Three-level synthetic strategy towards mixed-valence and heterometallic [2 2] gridlike arrays, Angew Chem Int Ed 43 **(2004)** 240-243.

5. J. Tan, M. Pan, S. Li, X. Yang, Two new Cd(II) coordination polymer based on Biphenyl-3, 3′, 5, 5′-tetracarboxylic acid, Inorg Chem Commun 87 **(2018)** 36-39.

6. K. C. Gupta, A. K. Sutar, Catalytic Activities of Schiff Base Transition Metal Complexes, Coord Chem Rev 252 **(2008)** 1420–1450.

7. Y. N. Belokon, W. Clegg, R. W. Harrington, M. North, C. Young, In situ formation of heterobimetallic salen complexes containing titanium and/or vanadium ions, Inorg Chem 47 **(2008)** 3801–3814.

8. N. Farrell, Transition Metal Complexes as Drugs and Chemotherapeutic Agents. Catalysis by Metal Complexes. 11 **(1989)**.

9. V. Balzani, A. Juris, M. Venturi, S. Campagna, S. Serroni, Luminescent and Redox-Active Polynuclear Transition Metal Complexes, Chem Rev 96 **(1996)** 759–833.

10. S. Xiang, D. X. Bao, J. Wang, Y. C. Li, X. Q. Zhao, Luminescent lanthanide coordination compounds with pyridine-2, 6-dicarboxylic acid, J Lumin 186 **(2017)** 273–282.

11. A. M. Baruah, A. Karmakar, A. K, Jubaraj B. Baruah, Hydrolytic ring opening reactions of anhydrides for first row transition metal dicarboxylate complexes, Polyhedron 26 **(2007)** 4518–4524

12. H. Aghabozorg, E. Sadr-khanlou, J. Soleimannejad, H. Adams, *Diaquabis(3*-carboxypyridine-2-carboxylato-κ2N,O2)zinc(II), Acta Crystallographica Section E Structure Reports Online, 63(6) **(2007)** m1769–m1769..

13. SMART V5.054, Bruker Analytical X-ray Systems, Madison,WI **(2001)**.

14. SAINT + V6.45, Bruker Analytical X-ray Systems, Madison,WI **(2001)**.

15. G. M. Sheldrick, Crystal Structure Refinement with SHELXL, Acta Cryst. C71 **(2015)** 3–8.

16. K. Momma, F. Izumi, VESTA 3 for Three-Dimensional Visualization of Crystal, Volumetric and Morphology Data, J. Appl. Cryst. 44 **(2011)** 1272-1276.

17. C. F. Macrae, P.R. Edgington, P. McCabe, E. Pidcock, G.P. Shields, R. Taylor, M. Towler, J. van de Streek, Mercury: Visualization and Analysis of Crystal Structures, J. Appl. Crystallogr. 39 **(2006)** 453–457.

18. N.K. Hansen, P. Coppens, Testing aspherical atom refinements on small-molecule data sets Acta Cryst. A 34 **(1978)** 909-921.

19. S. Domagala, B. Fournier, D. Liebschner, B. Guillot, C. Jelsch, An improved experimental databank of transferable multipolar atom models – ELMAM2. Construction details and applications, Acta Cryst. A68 **(2012)** 337-351.

20. F. H. Allen, The Cambridge Structural Database: a quarter of a million crystal structures and rising, Acta Cryst. B58 **(2002)** 380–388.

21. C. Jelsch, B. Guillot, A. Lagoutte, C. Lecomte, Advances in protein and small-molecule charge-density refinement methods using MoPro, J. Appl. Cryst. 38 **(2005)** 38-54.

22. B. Guillot, E. Enrique, L. Huder, C. Jelsch, MoProViewer: a tool to study proteins from a charge density science perspective, Acta Cryst. A70 **(2014)** C279.

23. C. T. Lee, W. T. Yang. R. G. Parr, Development of the Colle-Salvetti correlation-energy formula into a functional of the electron density, Phys. Rev B. 37 **(1988)** 785-789.

24. R. G. Parr and W. Yang, Density-Functional Theory of Atoms and Molecules (Oxford University Press, New York, **(1989)**.

25. A.D. Becke, Density-functional thermochemistry. III. The role of exact exchange, J. Chem. Phys., 98 **(1993)** 5648-5652.

26. M. Dolg, U. Wedig, H. Stoll, H. Preuss,Energy-adjusted ab initio pseudopotentials for the first row transition elements, J. Chem. Phys. 86 **(1987)** 866-872.

27. M. J. Frisch *et al.*, Gaussian 09 (Revision D.01), Gaussian Inc., Wallingford CT, **(2013)**.

28. R. Dennington, T. Keith and J. Millam, GaussView (Version 6), Semichem Inc., Shawnee Mission, KS, **(2016)**.

29. M. D. Hanwell, D. E. Curtis, D. C. Lonie, T. Vandermeersch, E. Zurek and G. R. Hutchison,Avogadro: an advanced semantic chemical editor, visualization, and analysis platform, J. Cheminform. 4 **(2012)** 17.

30. R. Pal, M. M. Reddy, B. Dinesh, M. A.Venkatesha, S. Grabowsky, C. Jelsch, T. N. Guru Row, Syn vs. Anti Carboxylic Acids in Hybrid Peptides: Experimental and Theoretical Charge Density and Chemical Bonding Analysis, J. Phys. Chem. A 122 **(2018)** 3665-3679.

31. C. Berríos, G. I. Cárdenas-Jirón, , J. F. Marco, C. Gutiérrez, , & M. S. Ureta-Zañartu,. Theoretical and spectroscopic study of nickel(II) porphyrin derivatives. J. Phys. Chem. A 111 **(2007)** 2706–2714.

32. R. Behjatmanesh-Ardakani, F. Pourroustaei-Ardakani, , M. Taghdiri, , & Z. M. Kotena, DFT-B3LYP study of interactions between host biphenyl-1-aza-18-crown-6 ether derivatives and guest Cd2+: NBO, NEDA, and QTAIM analyses. Journal of Molecular Modeling, 22(7) **(2016)** 149.

33. D. Dimić, M. Petković, Control of a photoswitching chelator by metal ions: DFT, NBO, and QTAIM analysis. International Journal of Quantum Chemistry, 116(1) **(2015)** 27–34.

34. S. M. Soliman, A. Barakat, M. S. Islam, H. A. Ghabbour, Synthesis, crystal structure and DFT studies of a new dinuclear Ag(I)-malonamide complex. Molecules, 23(4) **(2018)** 1–16.

35. S. M. Soliman, J. Albering, & M. A. M. Abu-Youssef, Structural analyses of two new highly distorted octahedral copper(II) complexes with quinoline-type ligands; Hirshfeld, AIM and NBO studies, Polyhedron 127 **(2017)** 36-50.

36. S. M. Soliman, Y. N. Mabkhot, A. Barakat, H. A. Ghabbour, A highly distorted hexacoordinated silver(I) complex: synthesis, crystal structure, and DFT studies. J Coord Chem 70 **(2017)** 1339–1356.

37. N. Smrečki, B. M. Kukovec, I. Rončević, & Z. Popović, New coordination modes of iminodiacetamide type ligands in palladium(II) complexes: crystallographic and DFT studies. Structural Chemistry, 29(1) **(2018)** 195–206.

38 C. Jelsch, S. Soudani, C. Ben Nasr, Likelihood of atom–atom contacts in crystal structures of halogenated organic compounds, IUCr J (**2015**) 2, 327-340**.**

39. L. Xiao-Hong, L. Xiang-Ru, Z. Xian-Zhou, Molecular structure and vibrational spectra of three substituted 4-thioflavones by density functional theory and ab initio Hartree-Fock calculations, Spectrochim. Acta Part A 78 **(2011)** 528-536.

40. A. Tokatlı, E. Ozen, F. Ucun, S. Bahçeli, Quantum chemical computational studies on 5-(4-bromophenylamino)-2-methylsulfanylmethyl-2H-1,2,3-triazol-4-carboxylic acid ethyl ester, Spectrochim. Acta A 78 **(2011)** 1201-1211.

41. E. Scrocco, J. Tomasi, Electronic molecular structure, reactivity and intermolecular forces: an euristic interpretation by means of electrostatic molecular potentials, Adv. Quant. Chem. 11 **(1978)** 115-193.

42. F.J. Luque, J.M. Lopez, M. Orozco, Perspective on electrostatic interactions of a solute with a continuum. A direct utilization of ab initio molecular potentials for the prevision of solvent effects, Theor. Chem. Acc. 103 **(2000)** 343-345.

43. N. Okulik, A.H. Jubert, Theoretical analysis of the reactive sites of non-esteroidal anti-inflammatory drugs, Int. Electron J. Mol. Des. 4 **(2005)** 17-30.

44. H. Saeidian, M. Sahandi, Comprehensive DFT study on molecular structures of lewisites in support of the chemical weapons convention, J. Mol. Struct. 1100 **(2015)** 486-495.

Table 1 Crystal data and structure parameters of the title compound

Crystal data	
Chemical formula	$C_{14}H_{12}N_2O_{10}Zn$
M_r	433.63
Crystal system, space group	Monoclinic, $P2_1/n$
Temperature (K)	193
a, b, c (Å)	9.2883 (17), 7.8953 (12), 10.3048 (19)
β (°)	95.070 (5)
V (Å^3)	752.7 (2)
Z	2
Radiation type	Mo $K\alpha$
μ (mm^{-1})	1.70
Crystal size (mm)	0.25 × 0.25 × 0.16
Data collection	
Diffractometer	Bruker Diffraction CCD area-detector
Absorption correction	Multi-scan *SMART* (Bruker, 2001)
T_{min}, T_{max}	0.736, 0.952
No. of measured, independent and observed [$I > 2\sigma(I)$] reflections	4473, 1815, 1710
R_{int}	0.019
$(\sin \theta/\lambda)_{max}$ (Å^{-1})	0.677
Refinement	
$R[F^2 > 2\sigma(F^2)]$, $wR(F^2)$, S	0.030, 0.090, 1.09
No. of reflections	1815
No. of parameters	133
No. of restraints	3
$\Delta\rho_{max}$, $\Delta\rho_{min}$ (e Å^{-3})	0.39, −0.32

Table 2 Bond lengths (Å) and bond angles (º) for non-H atoms with *esd* values in parenthesis of the title compound

Atoms	**Bond length**	**Atoms**	**Bond length**
Zn1—O2^{i}	2.0551 (13)	O5—C7	1.225 (2)
Zn1—O2	2.0551 (13)	N1—C1	1.328 (2)
Zn1—N1^{i}	2.0645 (15)	N1—C5	1.345 (2)
Zn1—N1	2.0646 (15)	C1—C2	1.379 (3)
Zn1—O1^{i}	2.1874 (15)	C2—C3	1.371 (3)
Zn1—O1	2.1874 (15)	C3—C4	1.397 (3)
O2—C6	1.245 (2)	C4—C5	1.398 (2)
O3—C6	1.256 (2)	C4—C7	1.525 (2)
O4—C7	1.281 (2)	C5—C6	1.538 (3)
O4—OH4	0.847 (18)		
Atoms	**Bond angle**	**Atoms**	**Bond angle**
O2^{i}—Zn1—O2	180.0	C5—N1—Zn1	116.07 (12)
O2^{i}—Zn1—N1^{i}	78.45 (6)	N1—C1—C2	121.84 (17)
O2—Zn1—N1^{i}	101.55 (6)	C3—C2—C1	117.85 (17)
O2^{i}—Zn1—N1	101.55 (6)	C2—C3—C4	121.45 (17)
O2—Zn1—N1	78.45 (6)	C3—C4—C5	117.18 (17)
N1^{i}—Zn1—N1	180.0	C3—C4—C7	114.17 (16)
O2^{i}—Zn1—O1^{i}	90.57 (5)	C5—C4—C7	128.65 (17)
O2—Zn1—O1^{i}	89.43 (6)	N1—C5—C4	120.51 (16)
N1^{i}—Zn1—O1^{i}	89.27 (6)	N1—C5—C6	111.12 (14)
N1—Zn1—O1^{i}	90.73 (6)	C4—C5—C6	128.38 (15)
O2^{i}—Zn1—O1	89.43 (5)	O2—C6—O3	122.50 (17)
O2—Zn1—O1	90.57 (5)	O2—C6—C5	117.61 (15)
N1^{i}—Zn1—O1	90.73 (6)	O3—C6—C5	119.89 (15)
N1—Zn1—O1	89.27 (6)	O5—C7—O4	120.64 (18)
O1^{i}—Zn1—O1	180.00 (4)	O5—C7—C4	118.77 (17)
Zn1—O1—OW1	106 (2)	O4—C7—C4	120.58 (17)
Zn1—O1—OW2	112.7 (19)	C7—O4—OH4	114 (2)
OW1—O1—OW2	114 (3)	C1—N1—C5	121.16 (16)
C6—O2—Zn1	116.50 (12)	C1—N1—Zn1	122.76 (12)

Symmetry code: (i) −*x*+1, −*y*+1, −*z*+1.

Table 3 Geometric details of hydrogen bond (Å, º) (D-donor; A-acceptor; H-hydrogen).

Interactions	**d(D—H)**	**d(H···A)**	**d(D···A)**	**<D—H···A**	**Symmetry code on atom A**
O1—OW1···O5	0.81	2.00	2.801 (2)	171 (3)	−*x*+ ½ , *y*−½, −*z*+$^{3}/_{2}$
O1—OW2···O5	0.81	2.04	2.840 (2)	173 (3)	*x*+1, *y*, *z*
O4—OH4···O3	0.85	1.55	2.394 (2)	174 (3)	*x*, *y*, *z*
C2—H2···O2	0.95	2.61	3.442 (2)	146(3)	*x*, *y*+1, *z*
C2—H2···O3	0.95	2.60	3.302 (2)	131	*x*, *y*+1, *z*

Table 4 Natural Atomic charges and electron configurations from the natural population analysis (NPA) [a].

Atom	Natural charge	Natural electron configuration
Zn	1.0596	[core]4S(0.37)3d(9.99)4p(0.56)5p(0.02)
O1	-0.7583	[core]2S(1.60)2p(5.15)3p(0.01)
O2	-0.6829	[core]2S(1.66)2p(5.02)
N1	-0.5261	[core]2S(1.32)2p(4.20)3p(0.01)

[a] Half of the data were presented due to symmetry consideration.

Table 5 The second order perturbative energies $E^{(2)}$ corresponding to donor-acceptor interactions between ligand donor orbitals (NBO(i)) and metal acceptor orbitals (NBO(j)).

Donor NBO(i)	Acceptor NBO(j)	$E^{(2)}$ (kcal/mol)
LP(1)O1	LP*(6)Zn	0.11
LP(1)O1	LP*(7)Zn	1.89
LP(1)O1	LP*(8)Zn	1.73
LP(1)O1	LP*(9)Zn	3.01
LP(2)O1	LP*(6)Zn	29.54
LP(2)O1	LP*(7)Zn	0.36
LP(2)O1	LP*(8)Zn	50.51
LP(2)O1	LP*(9)Zn	0.07
$E^{(2)}$: LP(O1) → LP*(Zn) = 87.22 kcal/mol		
LP(1)O2	LP*(6)Zn	6.50
LP(1)O2	LP*(7)Zn	13.16
LP(1)O2	LP*(9)Zn	7.18
LP(2)O2	LP*(6)Zn	45.56
LP(2)O2	LP*(7)Zn	56.38
LP(2)O2	LP*(8)Zn	0.58
LP(2)O2	LP*(9)Zn	5.86
LP(3)O2	LP*(6)Zn	0.35
LP(3)O2	LP*(7)Zn	0.51
LP(3)O2	LP*(8)Zn	8.04
$E^{(2)}$: LP(O2) → LP*(Zn) = 144.12 kcal/mol		
LP(1)N1	LP*(6)Zn	45.19
LP(1)N1	LP*(7)Zn	10.34
LP(1)N1	LP*(8)Zn	0.73
LP(1)N1	LP*(9)Zn	42.18
$E^{(2)}$: LP(N1) → LP*(Zn) = 98.44 kcal/mol		

LP: 1-center valence lone pair, *: Antibonding

Table 6 The hybridizations, occupancies and energies of the natural orbitals involved in the Zn–N and Zn–O interactions.

Orbital	Hybridization	Occupancy	Energy
LP(1)O1	s(10.48%) p 8.54(89.52%)	1.98466	-0.52038
LP(2)O1	s(24.15%) p 3.14(75.85%)	1.88275	-0.59282
LP(1)O2	s(38.29%) p 1.61(61.71%)	1.91442	-0.61364
LP(2)O2	s(20.48%) p 3.88(79.52%)	1.80087	-0.51223
LP(3)O2	s(0.00%) p 1.00(100.00%)	1.61113	-0.32133
LP(1)N1	s(23.27%) p 3.30(76.73%)	1.82515	-0.48309
LP*(6)Zn	s(99.84%) p 0.00(0.00%) d 0.00(0.16%)	0.36934	0.05221
LP*(7)Zn	s(0.00%) p 1.00(100.00%)	0.19409	0.26999
LP*(8)Zn	s(0.00%) p 1.00(100.00%)	0.18580	0.22614
LP*(9)Zn	s(0.00%) p 1.00(100.00%)	0.17865	0.23461

[b] The orbital occupancy (Electron density between 0 and 2)
[c] Energies are in atomic unit (1 a.u. = 627.5095 kcal/mol)
LP: 1-center valence lone pair, *: Antibonding

Table 7 QTAIM-topological properties at the Zn—N and Zn—O bond critical points (BCPs) [a].

Interaction	$\rho(e.a_0^{-3})$	$\nabla^2\rho(e.a_0^{-5})$	$G_c(a.u.)$	$V_c(a.u.)$	$\lvert V_c\rvert/G_c$	$H_c(a.u.)$	$E_{int}(kcal.mol^{-1})$
Zn—O1	0.03334	0.20592	0.06016	-0.06939	1.15342	-0.00923	-21.77144
Zn—O2	0.04687	0.37657	0.08618	-0.09492	1.10141	-0.00873	-29.78160
Zn—N	0.05415	0.42090	0.08963	-0.09416	1.05054	-0.00453	-29.54314

[a] Half of the data were presented due to symmetry consideration.

(ρ) Electron density, $(\nabla^2\rho)$ Laplacian of electron density, (G_c) Electron kinetic energy density, (V_c) Electron potential energy density, (H_c) Total electron energy density and E_{int} Interaction energy.

Table 8 Nature of intermolecular contacts on the Hirshfeld surface by chemical types. The second row contains the contribution S_x of each chemical type X on the Hirshfeld surface. The third part of the Table show the % C_{xy} of the contact types on the surface. The lower part of the Table shows the E_{xy} enrichment ratios of contact types. The major C_{xy} contact types and the E_{xy} ratios larger than unity (corresponding to the significantly enriched contacts) are highlighted in bold characters. The hydrophobic Hc atoms bound to carbon were distinguished from the more polar Ho water hydrogen atoms. Chemical types have been regrouped in hydrophobic (Hc and C) and charged atoms.

chem.	Zn	N	O	Ho	Hc	C
surf. %	9.8	3.9	31.4	13.9	15.5	25.5
Zn	0.0					
N	6.0	0.0			contacts	(%)
O	**13.1**	0.6	0.7			
Ho	1.7	0.3	**16.4**	0.3		
Hc	0.9	0.0	**15.1**	2.1	3.0	
C	2.2	0.0	**15.3**	8.0	6.2	8.2
Zn	0					
N	**7.1**	0			enrichment	
O	**1.77**	0.27	0.07			
Ho	0.48	0.33	**1.82**	0.15		
Hc	0.25	0	**1.61**	0.47	1.31	
C	0.38	0	1.03	1.14	0.86	**1.42**

Table 9 Nature of intermolecular contacts on the Hirshfeld surface if the metal complex formed by Zn(II) and two anions and two water molecules is considered as an entity. The major C_{xy} contact types and the E_{xy} ratios significantly larger than unities are highlighted in bold characters. The N and Zn chemical types, which are quasi absent from the entity surface are omitted.

chem.	O	Ho	Hc	C
surf %	31.8	17.4	19.0	31.3
O	1.1			
Ho	**21.5**	0.4	% contacts	
Hc	**18.4**	2.9	4.4	
C	**20.5**	10.1	8.5	10.9
O	0.1			
Ho	**1.9**	0.1	enrichment	
Hc	**1.5**	0.4	**1.2**	
C	1.1	0.9	0.7	**1.2**

Figures

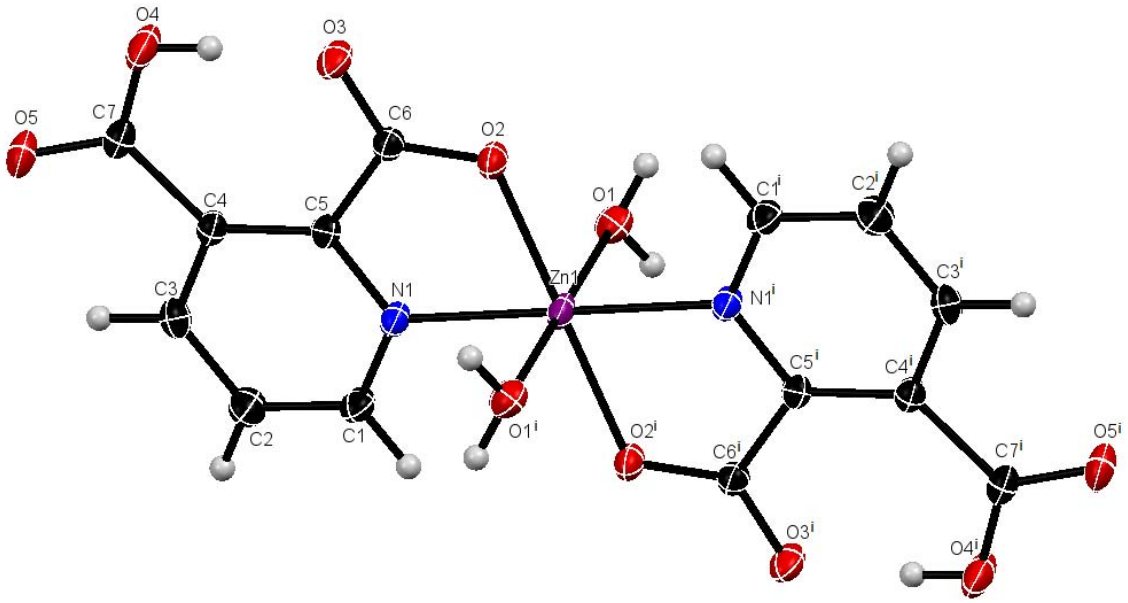

Fig. 1 Structure of [Zn(2,3—pdcH)$_2$(H$_2$O)$_2$]

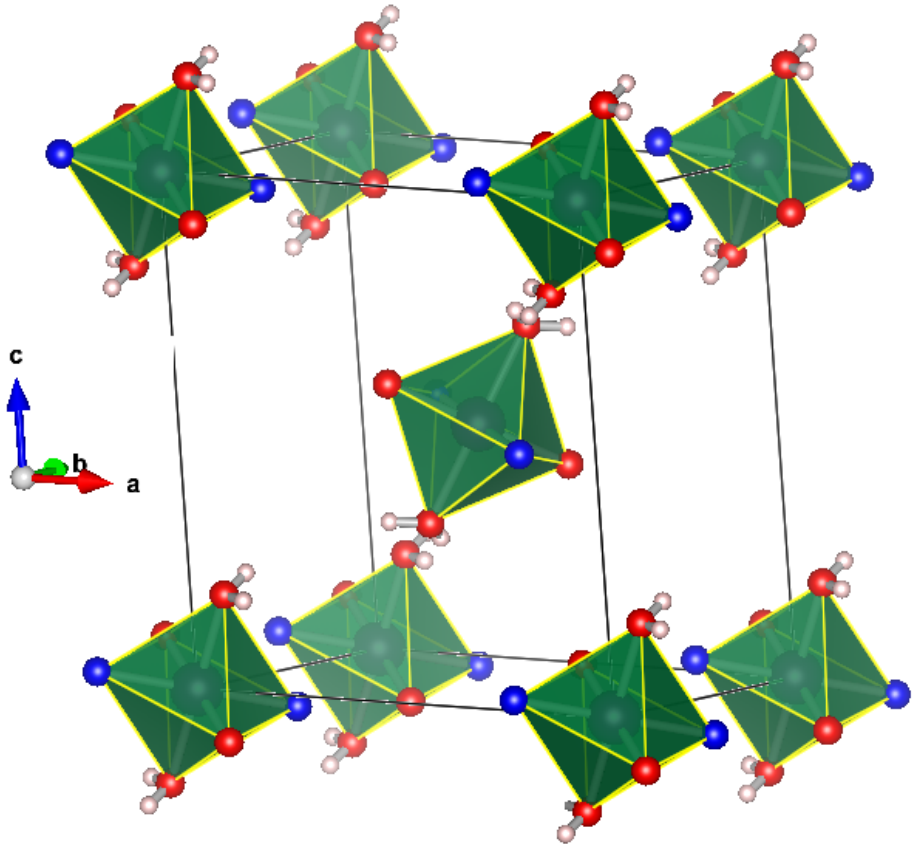

Fig. 2 Coordination environment of the Zn(II) atom with atomic labels in the title compound

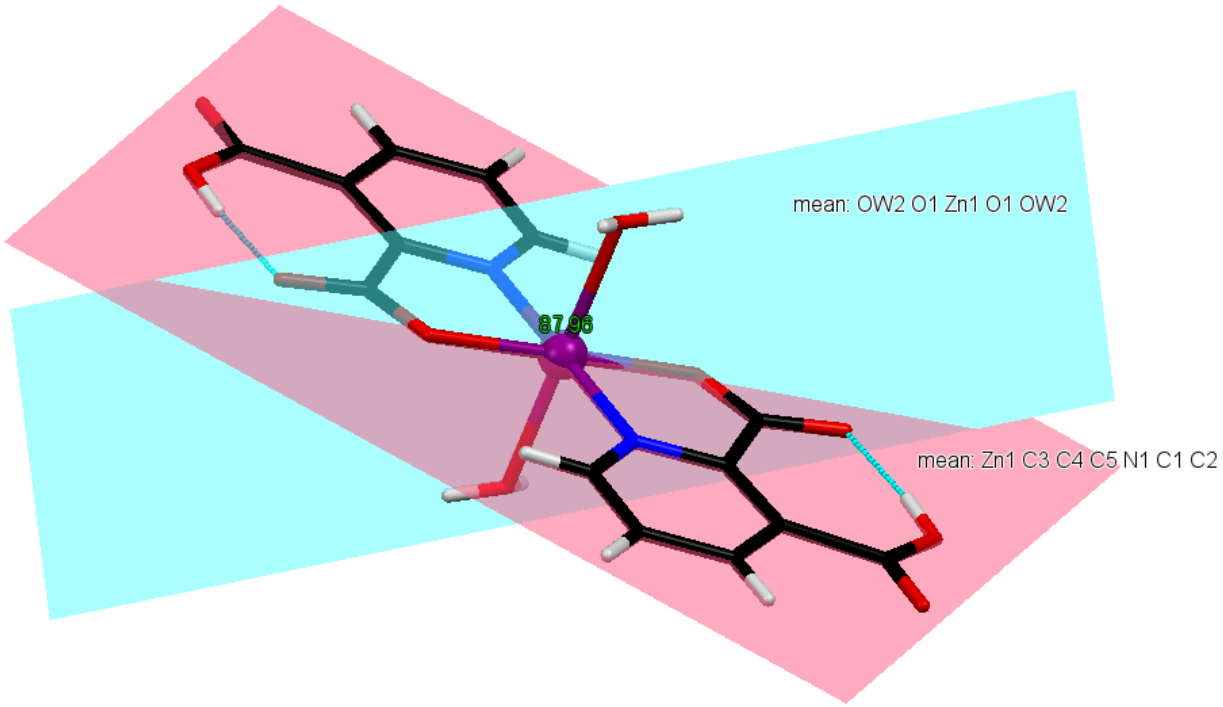

Fig. 3 Dihedral angle between the planes of water molecules and the pyridine dicarboxylic acid in the title compound

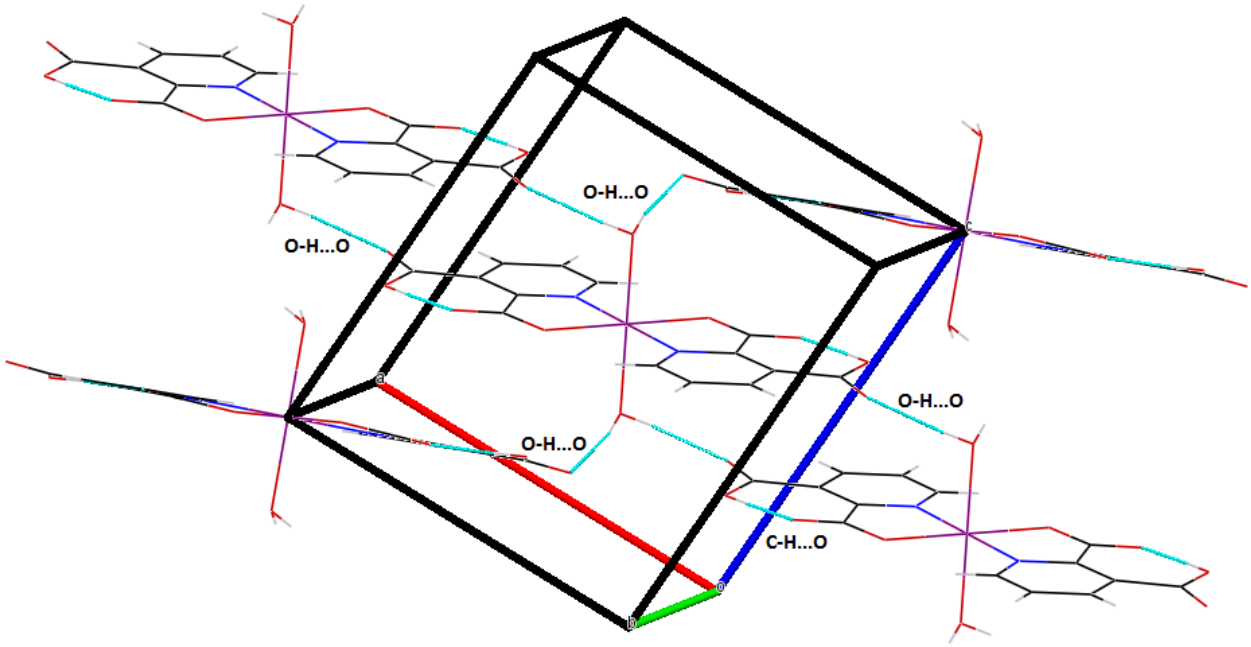

Fig. 4 The $[Zn(2,3\text{-pdcH})_2(H_2O)_2]$ entities and the neighbouring moieties in the title compound

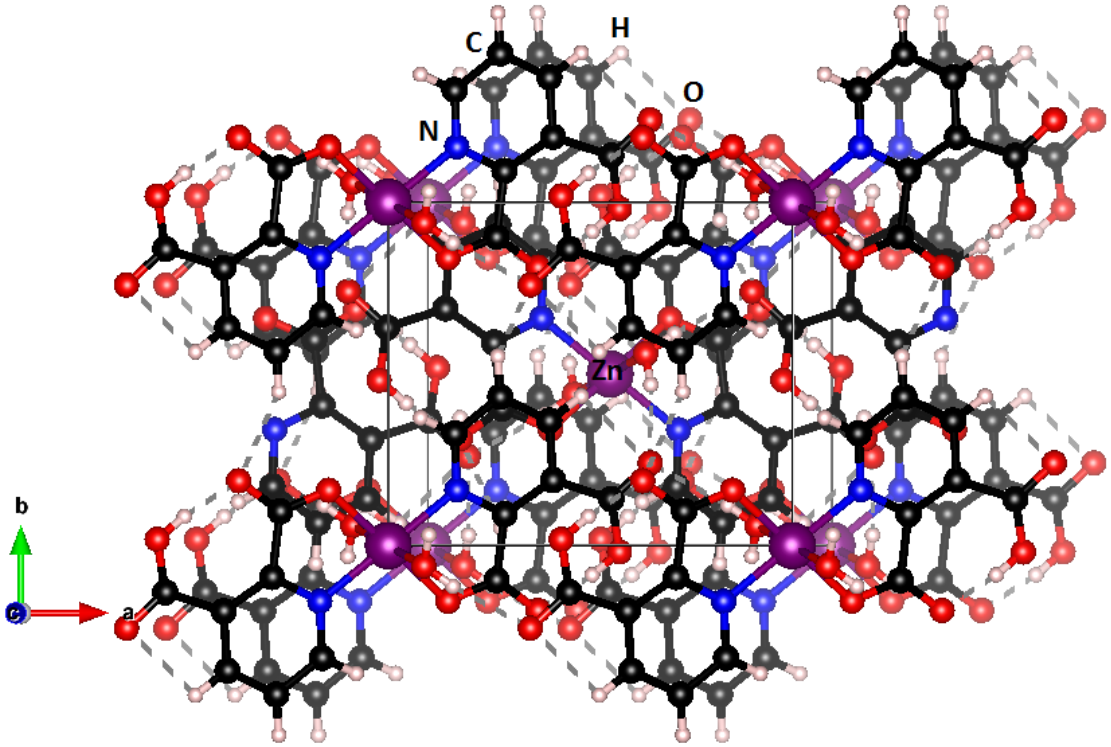

Fig. 5 View of the three-dimensional supramolecular structure of the title compound along the **c** axis, incorporating hydrogen bonds (dashed lines).

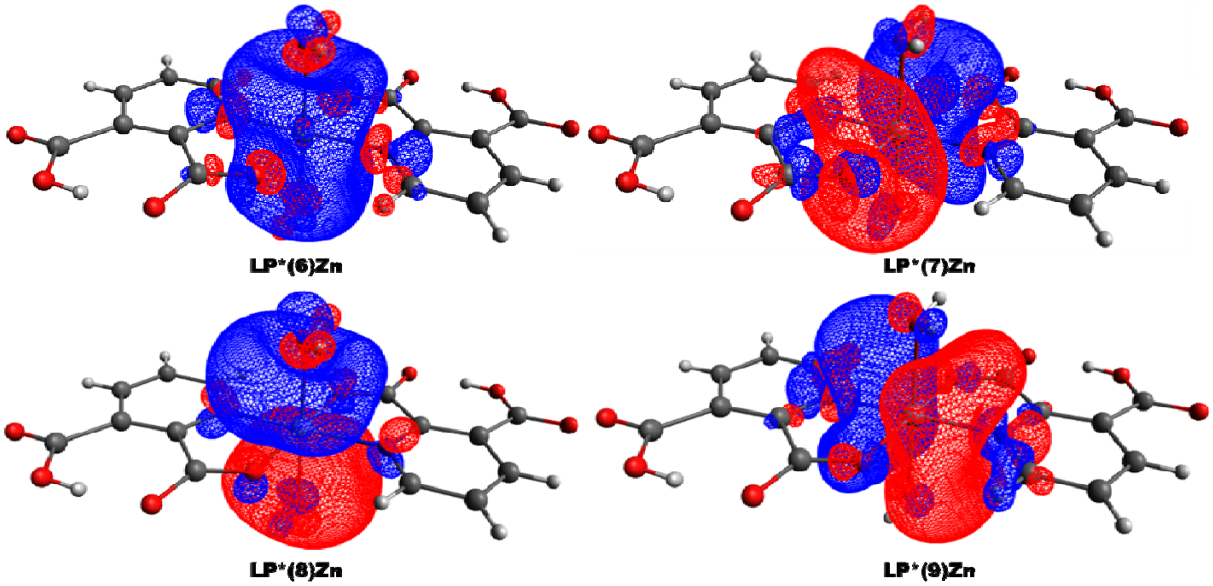

Fig. 6 Visualization of the anti-bonding natural orbitals of Zn cation shared in the O/N → Zn interactions.

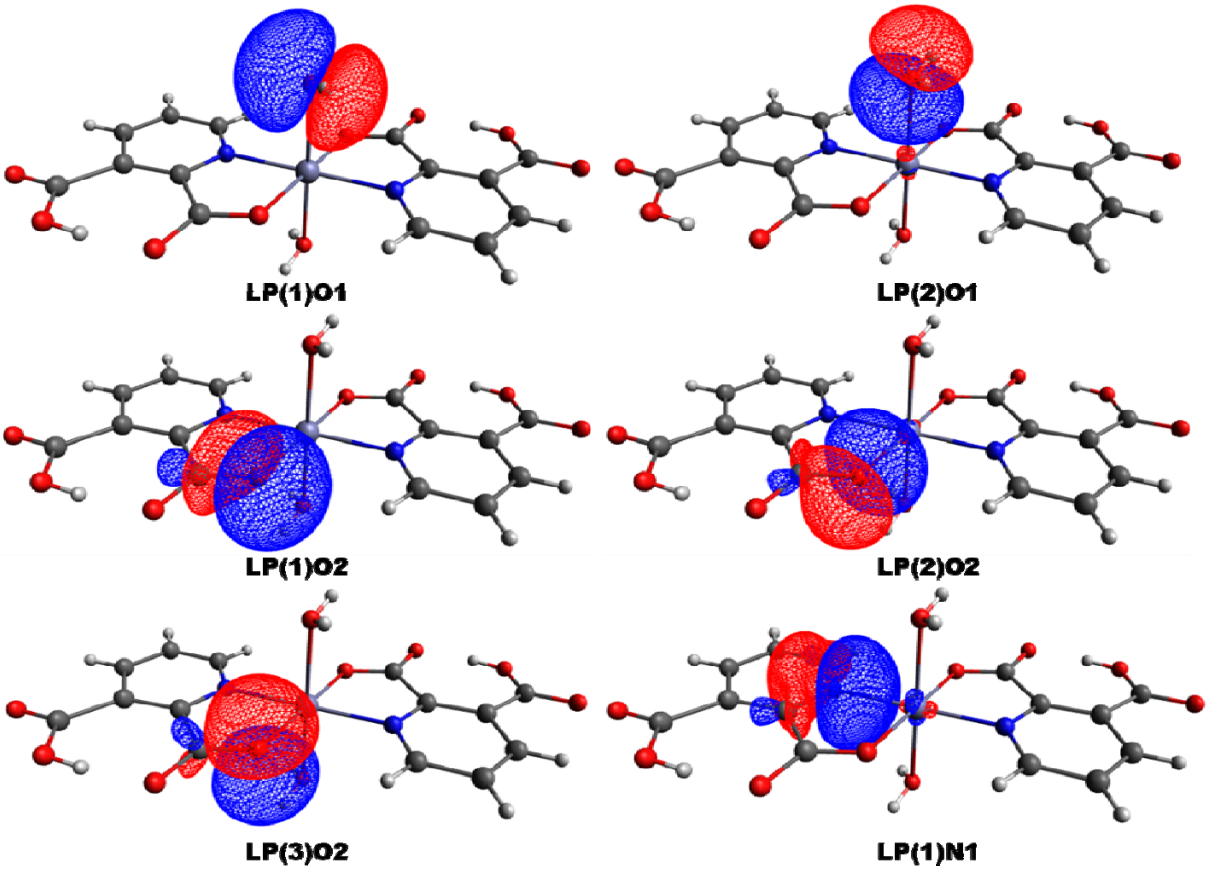

Fig. 7 Visualisation of the non-bonding natural orbitals of the O and N ligand donor atoms shared in the O/N → Zn interactions

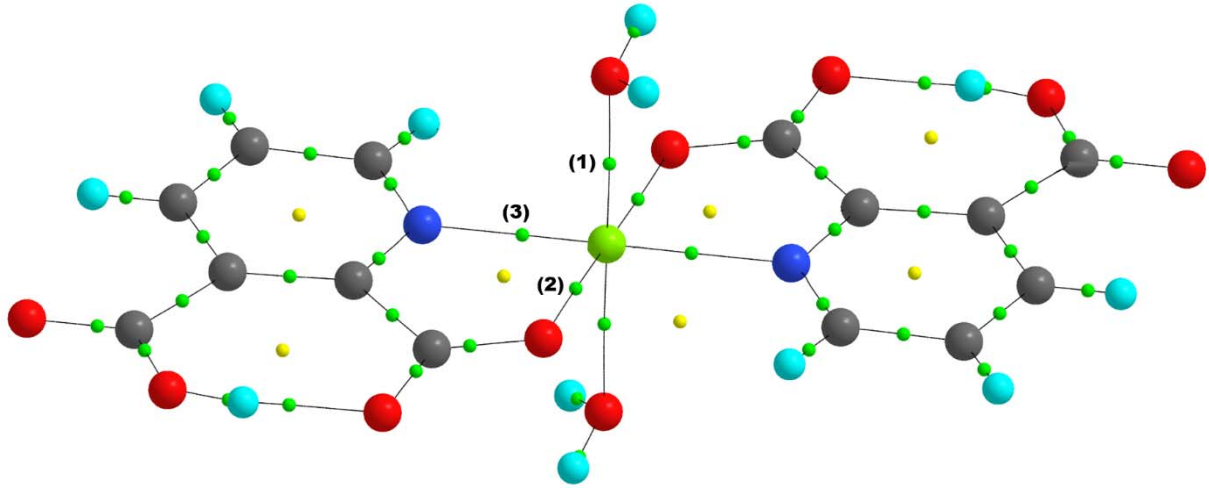

Fig. 8 QTAIM molecular graph for complex **1**: bond critical points (small green spheres), ring critical points (small yellow sphere) and bond paths (black lines).

(a)

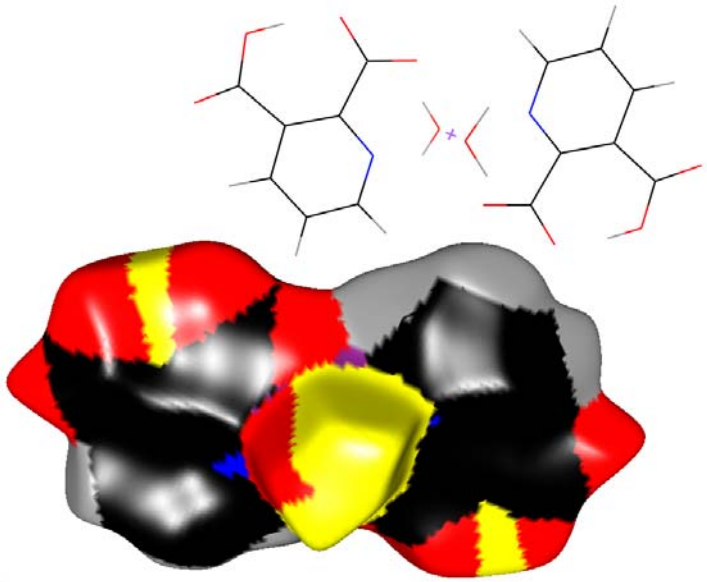

(b)

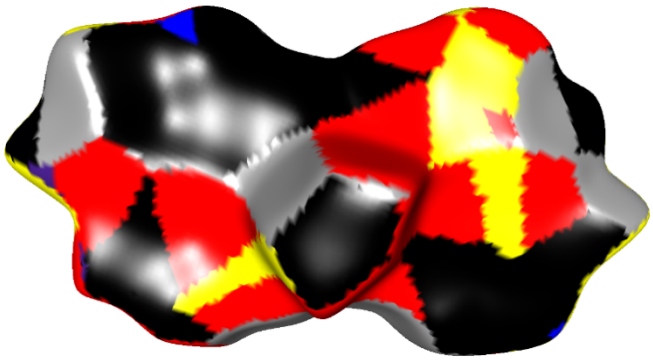

Fig. 9 Hirshfeld surface around the (Zn(II), 2HOH, 2 anions) complex. (a) coloured according to interior atom contributing most to the electron density (b) according to the exterior atom. Carbon: black, hydrogen Hc: grey, hydrogen Ho: yellow, oxygen: red, nitrogen: blue, zinc: purple. The orientation of the complex is also represented in (a).

(a)
(b)

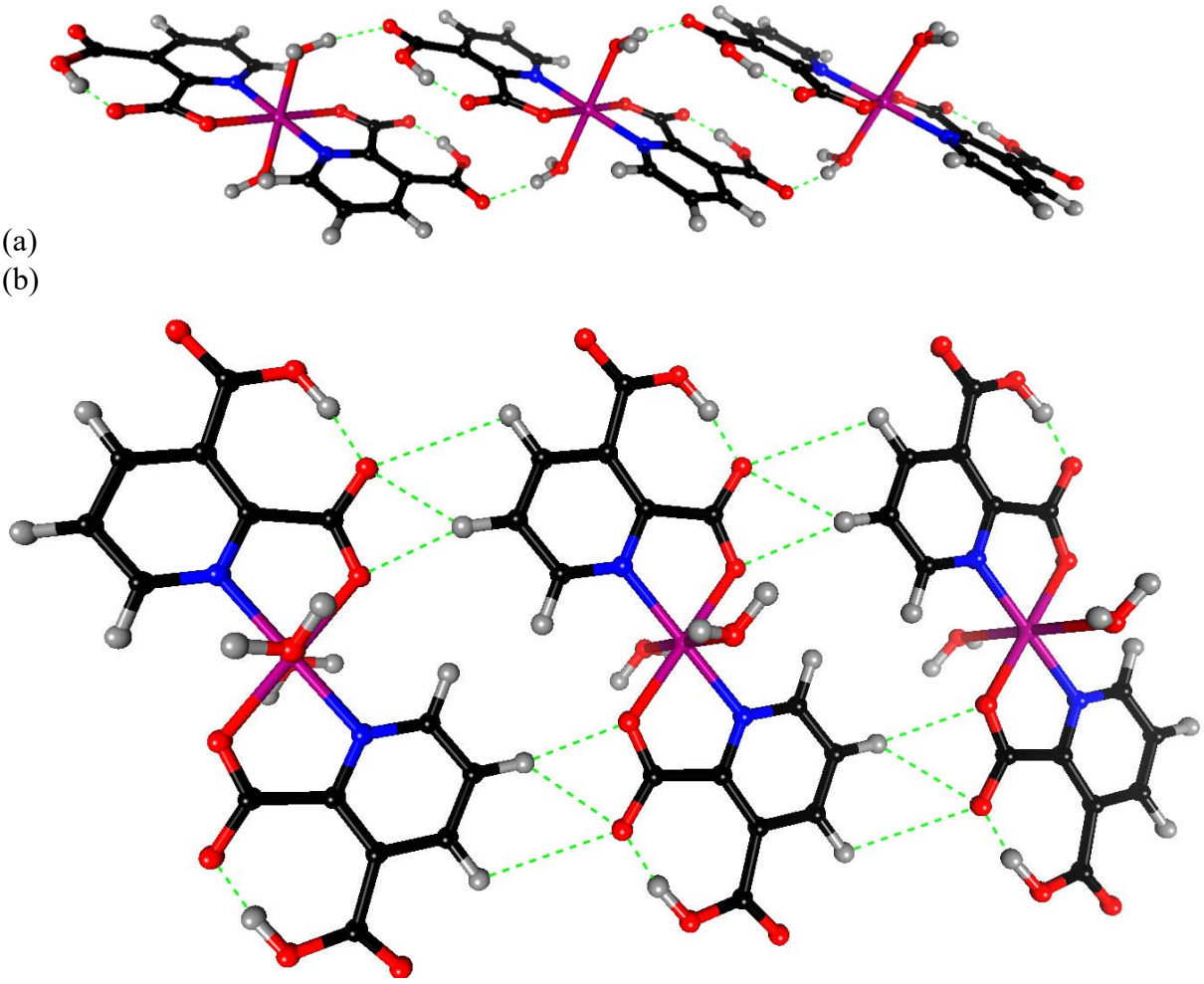

Fig. 10 Crystallographic autostereogram of a dimer of the asymmetric unit. The figure was done with MoProViewer. Hydrogen bonds are represented as green dotted lines;

(a) The molecules are translated along vector **a**.

(b) The molecules are translated along vector **b**.

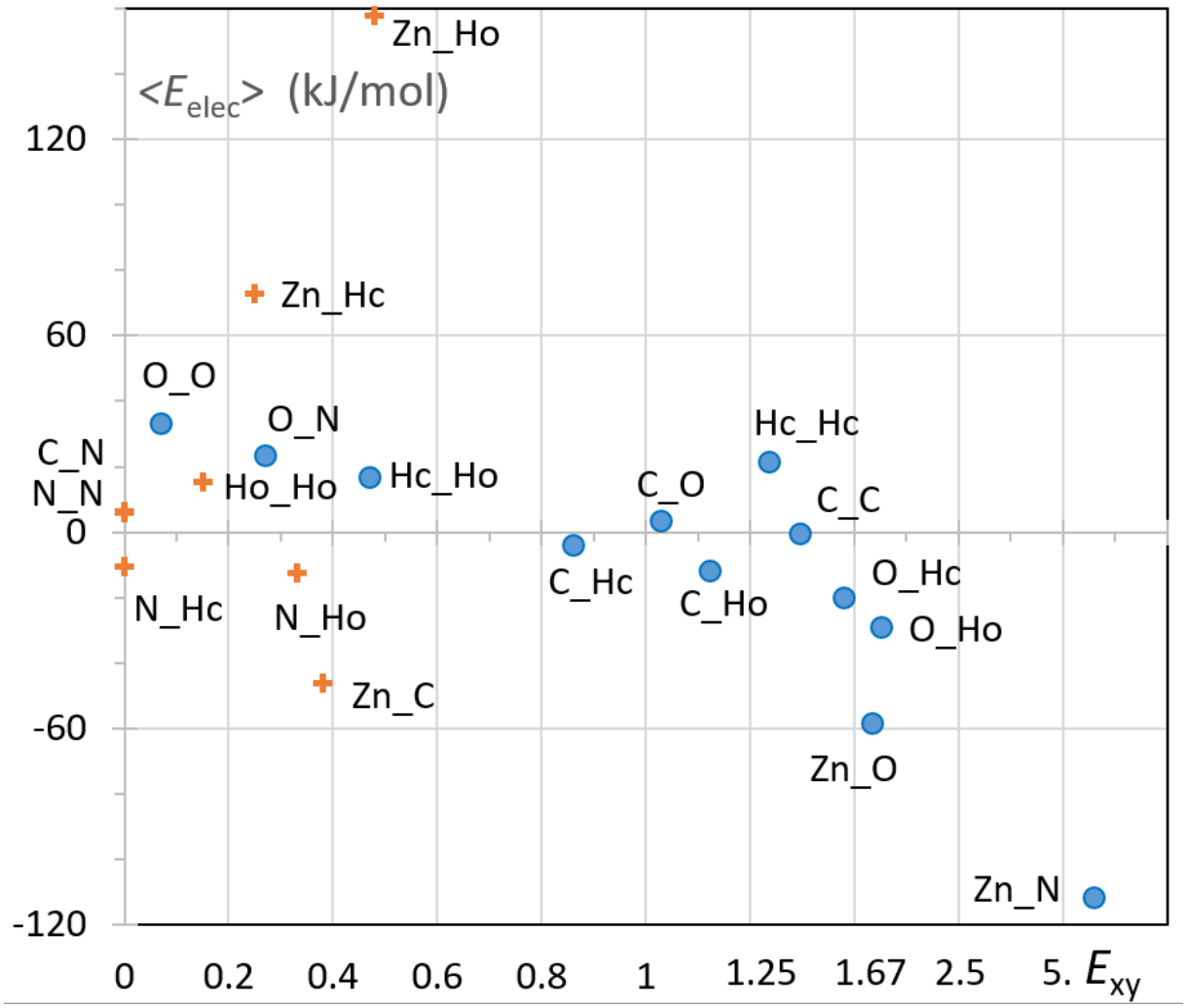

Fig. 11 Scatterplot of average electrostatic energy $\langle E_{elec} \rangle$ vs. enrichment ratios E_{xy} for the different contact types. The E_{elec} values were averaged over the contacts which are shorter than the sum of van der Waals radii plus 0.2 Å. The orange crosses are contacts which are not observed in the crystal packing at this cutoff distance. Their theoretical E_{elec} values were computed between two atoms rendered spherical (with multipoles removed) and placed at this cutoff distance.

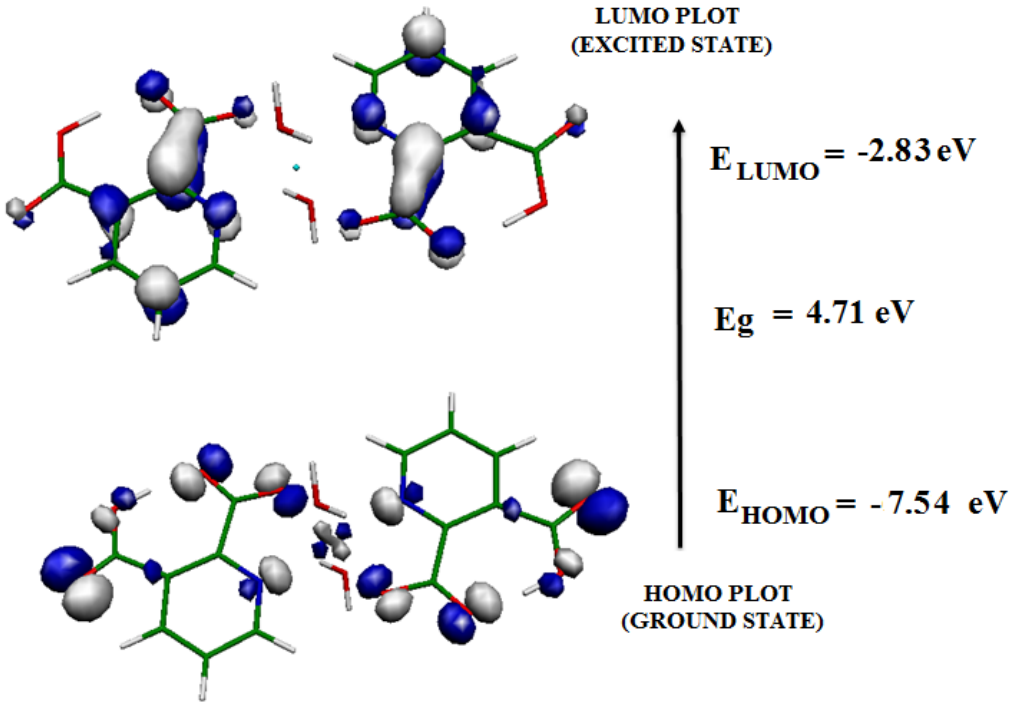

Fig. 12 Frontier molecular orbitals (HOMO and LUMO) of the title compound.

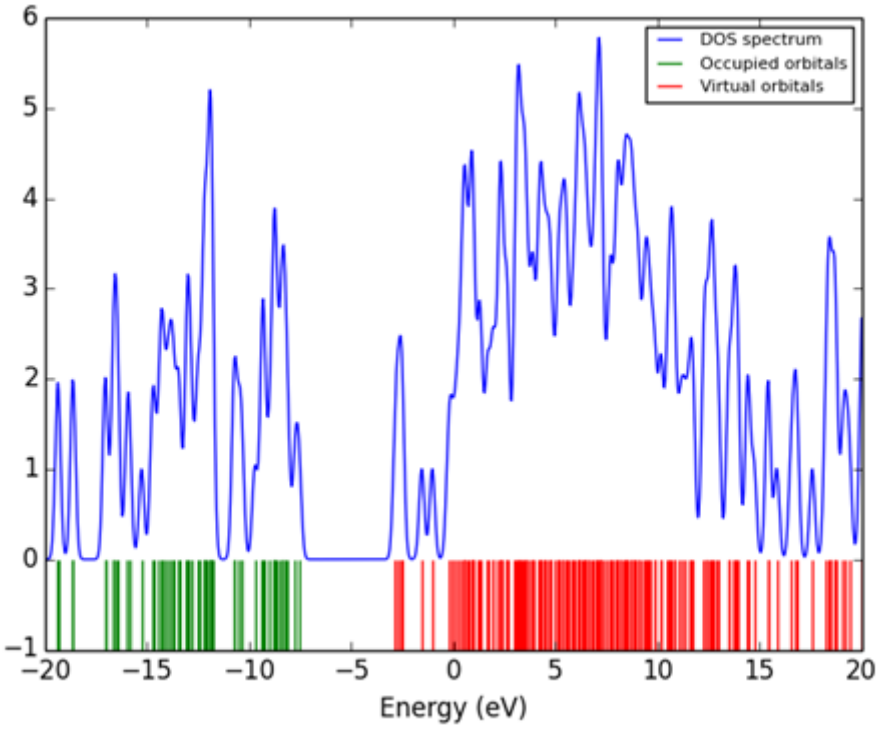

Fig. 13 DSO Spectrum and its energy levels of the Frontier Molecular Orbitals.

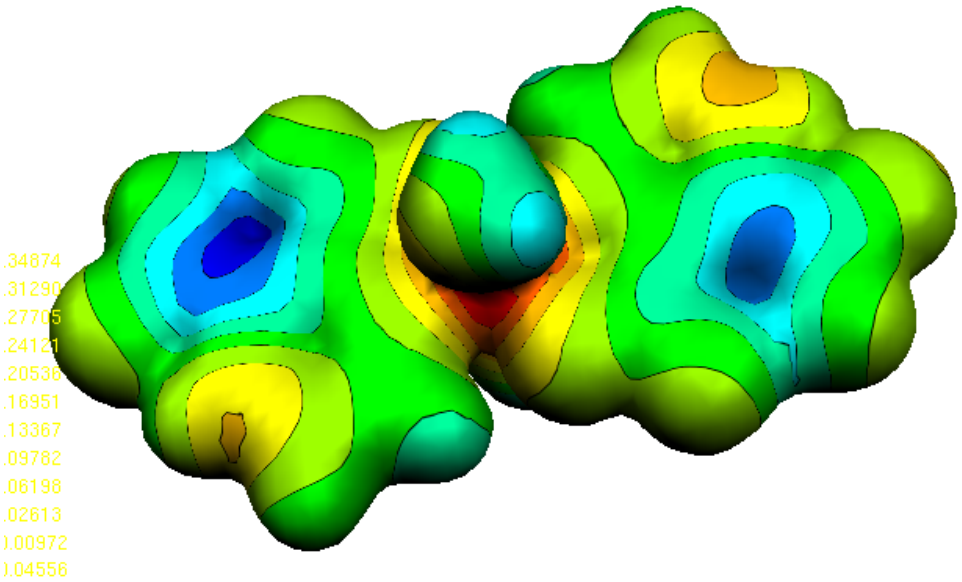

Fig. 14 Molecular electrostatic potential (MEP) of the title compound.

Supplement: CIF FILE.

```
_audit_creation_method          SHELXL-2013
_chemical_name_systematic
;
 ?
;
_chemical_name_common            ?
_chemical_melting_point          ?
_chemical_formula_moiety         ?
_chemical_formula_sum
'C14 H12 N2 O10 Zn'
_chemical_formula_weight         433.63

loop_
 _atom_type_symbol
 _atom_type_description
 _atom_type_scat_dispersion_real
 _atom_type_scat_dispersion_imag
 _atom_type_scat_source
'C'  'C'   0.0033   0.0016
'International Tables Vol C Tables 4.2.6.8 and 6.1.1.4'
'N'  'N'   0.0061   0.0033
'International Tables Vol C Tables 4.2.6.8 and 6.1.1.4'
'O'  'O'   0.0106   0.0060
'International Tables Vol C Tables 4.2.6.8 and 6.1.1.4'
'H'  'H'   0.0000   0.0000
```

'International Tables Vol C Tables 4.2.6.8 and 6.1.1.4'
'Zn' 'Zn' 0.2839 1.4301
'International Tables Vol C Tables 4.2.6.8 and 6.1.1.4'

_space_group_crystal_system monoclinic
_space_group_IT_number 14
_space_group_name_H-M_alt 'P 21/n'
_space_group_name_Hall '-P 2yn'

_shelx_space_group_comment
;
The symmetry employed for this shelxl refinement is uniquely defined
by the following loop, which should always be used as a source of
symmetry information in preference to the above space-group names.
They are only intended as comments.
;

loop_
_space_group_symop_operation_xyz
'x, y, z'
'-x+1/2, y+1/2, -z+1/2'
'-x, -y, -z'
'x-1/2, -y-1/2, z-1/2'

_cell_length_a 9.2883(17)
_cell_length_b 7.8953(12)
_cell_length_c 10.3048(19)
_cell_angle_alpha 90
_cell_angle_beta 95.070(5)
_cell_angle_gamma 90
_cell_volume 752.7(2)
_cell_formula_units_Z 2
_cell_measurement_temperature 193(2)
_cell_measurement_reflns_used 4473
_cell_measurement_theta_min 2.831
_cell_measurement_theta_max 28.742

_exptl_crystal_description 'prism'
_exptl_crystal_colour 'whrite'
_exptl_crystal_density_meas ?
_exptl_crystal_density_method ?
_exptl_crystal_density_diffrn 1.913
_exptl_crystal_F_000 440
_exptl_transmission_factor_min ?
_exptl_transmission_factor_max ?
_exptl_crystal_size_max 0.250
_exptl_crystal_size_mid 0.250
_exptl_crystal_size_min 0.160
_exptl_absorpt_coefficient_mu 1.699
_shelx_estimated_absorpt_T_min 0.676
_shelx_estimated_absorpt_T_max 0.773
_exptl_absorpt_correction_type multi-scan
_exptl_absorpt_correction_T_min 0.736
_exptl_absorpt_correction_T_max 0.952
_exptl_absorpt_process_details 'SMART (Bruker, 2001)'

```
_exptl_special_details
;
 ?

;

_diffrn_ambient_temperature       193(2)
_diffrn_radiation_wavelength      0.71073
_diffrn_radiation_type            MoK\a
_diffrn_measurement_device_type   'Bruker Diffraction CCD area-detector'
_diffrn_measurement_method
'1265 images,\f=0, 90, 180 degree, and \D\w=0.3 degree, \c= 54.74 degree'
_diffrn_detector_area_resol_mean  .
_diffrn_standards_number          0
_diffrn_standards_interval_count  .
_diffrn_standards_interval_time   .
_diffrn_standards_decay_%         .
_diffrn_reflns_number             4473
_diffrn_reflns_av_unetI/netI      0.0238
_diffrn_reflns_av_R_equivalents   0.0191
_diffrn_reflns_limit_h_min        -12
_diffrn_reflns_limit_h_max        12
_diffrn_reflns_limit_k_min        -10
_diffrn_reflns_limit_k_max        6
_diffrn_reflns_limit_l_min        -12
_diffrn_reflns_limit_l_max        13
_diffrn_reflns_theta_min          2.831
_diffrn_reflns_theta_max          28.742
_diffrn_reflns_theta_full         25.242
_diffrn_measured_fraction_theta_max   0.929
_diffrn_measured_fraction_theta_full  0.997
_diffrn_reflns_Laue_measured_fraction_max    0.929
_diffrn_reflns_Laue_measured_fraction_full   0.997
_diffrn_reflns_point_group_measured_fraction_max   0.929
_diffrn_reflns_point_group_measured_fraction_full  0.997
_reflns_number_total              1815
_reflns_number_gt                 1710
_reflns_threshold_expression      'I > 2\s(I)'
_reflns_Friedel_coverage          0.000
_reflns_Friedel_fraction_max      .
_reflns_Friedel_fraction_full     .

_reflns_special_details
;
 Reflections were merged by SHELXL according to the crystal
 class for the calculation of statistics and refinement.

 _reflns_Friedel_fraction is defined as the number of unique
 Friedel pairs measured divided by the number that would be
 possible theoretically, ignoring centric projections and
 systematic absences.
;
```

```
_computing_data_collection        'SMART (Bruker, 2001)'
_computing_cell_refinement        'SAINT (Bruker, 2001)'
_computing_data_reduction         'SAINT (Bruker, 2001)'
_computing_structure_solution     'SHELXS-2013 (Sheldrick, 2015)'
_computing_structure_refinement   'SHELXL-2013 (Sheldrick, 2015)'
_computing_molecular_graphics
'DIAMOND (Brandenburg, 2011) and ATOMS (Dowty, 2004)'
_computing_publication_material
'SHELXL-2013 (Sheldrick, 2015)'

_refine_special_details
;
 ?
;
_refine_ls_structure_factor_coef  Fsqd
_refine_ls_matrix_type            full
_refine_ls_weighting_scheme       calc
_refine_ls_weighting_details
;
 w=1/[\s^2^(Fo^2^)+(0.0487P)^2^+0.4659P]
 where P=(Fo^2^+2Fc^2^)/3
;
_atom_sites_solution_primary      'Direct method'
_atom_sites_solution_secondary     ?
_atom_sites_solution_hydrogens    mixed
_refine_ls_hydrogen_treatment     mixed
_refine_ls_extinction_method      none
_refine_ls_extinction_coef        .
_refine_ls_number_reflns          1815
_refine_ls_number_parameters      133
_refine_ls_number_restraints      3
_refine_ls_R_factor_all           0.0318
_refine_ls_R_factor_gt            0.0298
_refine_ls_wR_factor_ref          0.0898
_refine_ls_wR_factor_gt           0.0877
_refine_ls_goodness_of_fit_ref    1.094
_refine_ls_restrained_S_all       1.094
_refine_ls_shift/su_max           0.000
_refine_ls_shift/su_mean          0.000

loop_
 _atom_site_label
 _atom_site_type_symbol
 _atom_site_fract_x
 _atom_site_fract_y
 _atom_site_fract_z
 _atom_site_U_iso_or_equiv
 _atom_site_adp_type
 _atom_site_occupancy
 _atom_site_site_symmetry_order
 _atom_site_calc_flag
 _atom_site_refinement_flags_posn
 _atom_site_refinement_flags_adp
 _atom_site_refinement_flags_occupancy
 _atom_site_disorder_assembly
```

```
 _atom_site_disorder_group
Zn1 Zn 0.5000 0.5000 0.5000 0.01852(13) Uani 1 2 d S . P . .
O1 O 0.60678(15) 0.5590(2) 0.69242(14) 0.0233(3) Uani 1 1 d D . . . .
OW1 H 0.623(3) 0.469(3) 0.729(3) 0.035 Uiso 1 1 d D U . . .
OW2 H 0.678(2) 0.618(3) 0.689(3) 0.035 Uiso 1 1 d D U . . .
O2 O 0.36037(14) 0.33848(17) 0.58238(14) 0.0199(3) Uani 1 1 d . . . . .
O3 O 0.14420(15) 0.31122(17) 0.64968(14) 0.0236(3) Uani 1 1 d . . . . .
O4 O -0.05121(19) 0.48168(19) 0.71248(19) 0.0312(4) Uani 1 1 d D . . . .
OH4 H 0.014(3) 0.415(3) 0.691(3) 0.047 Uiso 1 1 d D U . . .
O5 O -0.12979(14) 0.74053(19) 0.68779(15) 0.0258(3) Uani 1 1 d . . . . .
N1 N 0.33401(16) 0.6621(2) 0.53686(15) 0.0167(3) Uani 1 1 d . . . . .
C1 C 0.3372(2) 0.8269(2) 0.51146(19) 0.0205(4) Uani 1 1 d . . . . .
H1 H 0.4177 0.8725 0.4726 0.025 Uiso 1 1 calc R U . . .
C2 C 0.2269(2) 0.9337(2) 0.5400(2) 0.0234(4) Uani 1 1 d . . . . .
H2 H 0.2311 1.0517 0.5226 0.028 Uiso 1 1 calc R U . . .
C3 C 0.1109(2) 0.8642(2) 0.59407(18) 0.0206(4) Uani 1 1 d . . . . .
H3 H 0.0336 0.9354 0.6144 0.025 Uiso 1 1 calc R U . . .
C4 C 0.10391(19) 0.6908(2) 0.61996(17) 0.0162(3) Uani 1 1 d . . . . .
C5 C 0.22116(18) 0.5915(2) 0.58998(16) 0.0153(3) Uani 1 1 d . . . . .
C6 C 0.24301(19) 0.3998(2) 0.60884(17) 0.0164(3) Uani 1 1 d . . . . .
C7 C -0.03444(19) 0.6356(2) 0.67729(18) 0.0195(4) Uani 1 1 d . . . . .

loop_
 _atom_site_aniso_label
 _atom_site_aniso_U_11
 _atom_site_aniso_U_22
 _atom_site_aniso_U_33
 _atom_site_aniso_U_23
 _atom_site_aniso_U_13
 _atom_site_aniso_U_12
Zn1 0.01279(18) 0.01647(19) 0.0275(2) 0.00102(10) 0.00827(12) 0.00127(10)
O1 0.0179(7) 0.0257(8) 0.0267(7) 0.0025(6) 0.0042(5) -0.0034(6)
O2 0.0157(6) 0.0160(6) 0.0288(7) 0.0018(5) 0.0071(5) 0.0024(5)
O3 0.0187(7) 0.0178(7) 0.0357(8) 0.0026(6) 0.0102(6) -0.0012(5)
O4 0.0208(8) 0.0249(8) 0.0507(10) 0.0046(7) 0.0192(7) 0.0029(6)
O5 0.0144(6) 0.0278(7) 0.0362(8) -0.0046(6) 0.0076(5) 0.0019(5)
N1 0.0133(7) 0.0164(7) 0.0209(7) -0.0005(6) 0.0044(6) 0.0000(5)
C1 0.0183(9) 0.0175(9) 0.0267(9) 0.0020(7) 0.0069(7) -0.0013(7)
C2 0.0247(10) 0.0158(9) 0.0302(10) 0.0013(7) 0.0054(8) 0.0018(7)
C3 0.0193(9) 0.0182(9) 0.0245(9) -0.0008(7) 0.0034(7) 0.0060(7)
C4 0.0135(8) 0.0191(8) 0.0162(8) -0.0009(7) 0.0017(6) 0.0004(6)
C5 0.0128(8) 0.0166(8) 0.0166(8) -0.0010(6) 0.0009(6) -0.0003(6)
C6 0.0155(8) 0.0165(8) 0.0174(8) -0.0002(6) 0.0026(6) 0.0004(6)
C7 0.0139(8) 0.0244(9) 0.0204(8) -0.0033(7) 0.0029(6) -0.0003(7)

_geom_special_details
;
 All esds (except the esd in the dihedral angle between two l.s. planes)
 are estimated using the full covariance matrix.  The cell esds are taken
 into account individually in the estimation of esds in distances, angles
 and torsion angles; correlations between esds in cell parameters are only
 used when they are defined by crystal symmetry.  An approximate (isotropic)
 treatment of cell esds is used for estimating esds involving l.s. planes.
;
```

```
loop_
 _geom_bond_atom_site_label_1
 _geom_bond_atom_site_label_2
 _geom_bond_distance
 _geom_bond_site_symmetry_2
 _geom_bond_publ_flag
Zn1 O2 2.0551(13) 3_666 ?
Zn1 O2 2.0551(13) . ?
Zn1 N1 2.0645(15) 3_666 ?
Zn1 N1 2.0646(15) . ?
Zn1 O1 2.1874(15) 3_666 ?
Zn1 O1 2.1874(15) . ?
O1 OW1 0.814(17) . ?
O1 OW2 0.808(17) . ?
O2 C6 1.245(2) . ?
O3 C6 1.256(2) . ?
O4 C7 1.281(2) . ?
O4 OH4 0.847(18) . ?
O5 C7 1.225(2) . ?
N1 C1 1.328(2) . ?
N1 C5 1.345(2) . ?
C1 C2 1.379(3) . ?
C1 H1 0.9500 . ?
C2 C3 1.371(3) . ?
C2 H2 0.9500 . ?
C3 C4 1.397(3) . ?
C3 H3 0.9500 . ?
C4 C5 1.398(2) . ?
C4 C7 1.525(2) . ?
C5 C6 1.538(3) . ?

loop_
 _geom_angle_atom_site_label_1
 _geom_angle_atom_site_label_2
 _geom_angle_atom_site_label_3
 _geom_angle
 _geom_angle_site_symmetry_1
 _geom_angle_site_symmetry_3
 _geom_angle_publ_flag
O2 Zn1 O2 180.0 3_666 . ?
O2 Zn1 N1 78.45(6) 3_666 3_666 ?
O2 Zn1 N1 101.55(6) . 3_666 ?
O2 Zn1 N1 101.55(6) 3_666 . ?
O2 Zn1 N1 78.45(6) . . ?
N1 Zn1 N1 180.0 3_666 . ?
O2 Zn1 O1 90.57(5) 3_666 3_666 ?
O2 Zn1 O1 89.43(6) . 3_666 ?
N1 Zn1 O1 89.27(6) 3_666 3_666 ?
N1 Zn1 O1 90.73(6) . 3_666 ?
O2 Zn1 O1 89.43(5) 3_666 . ?
O2 Zn1 O1 90.57(5) . . ?
N1 Zn1 O1 90.73(6) 3_666 . ?
N1 Zn1 O1 89.27(6) . . ?
O1 Zn1 O1 180.00(4) 3_666 . ?
Zn1 O1 OW1 106(2) . . ?
```

```
Zn1 O1 OW2 112.7(19) . . ?
OW1 O1 OW2 114(3) . . ?
C6 O2 Zn1 116.50(12) . . ?
C7 O4 OH4 114(2) . . ?
C1 N1 C5 121.16(16) . . ?
C1 N1 Zn1 122.76(12) . . ?
C5 N1 Zn1 116.07(12) . . ?
N1 C1 C2 121.84(17) . . ?
N1 C1 H1 119.1 . . ?
C2 C1 H1 119.1 . . ?
C3 C2 C1 117.85(17) . . ?
C3 C2 H2 121.1 . . ?
C1 C2 H2 121.1 . . ?
C2 C3 C4 121.45(17) . . ?
C2 C3 H3 119.3 . . ?
C4 C3 H3 119.3 . . ?
C3 C4 C5 117.18(17) . . ?
C3 C4 C7 114.17(16) . . ?
C5 C4 C7 128.65(17) . . ?
N1 C5 C4 120.51(16) . . ?
N1 C5 C6 111.12(14) . . ?
C4 C5 C6 128.38(15) . . ?
O2 C6 O3 122.50(17) . . ?
O2 C6 C5 117.61(15) . . ?
O3 C6 C5 119.89(15) . . ?
O5 C7 O4 120.64(18) . . ?
O5 C7 C4 118.77(17) . . ?
O4 C7 C4 120.58(17) . . ?

loop_
 _geom_hbond_atom_site_label_D
 _geom_hbond_atom_site_label_H
 _geom_hbond_atom_site_label_A
 _geom_hbond_distance_DH
 _geom_hbond_distance_HA
 _geom_hbond_distance_DA
 _geom_hbond_angle_DHA
 _geom_hbond_site_symmetry_A
O1 OW1 O5  0.814(17) 1.995(17) 2.801(2) 171(3) 2_546
O1 OW2 O5  0.808(17) 2.036(18) 2.840(2) 173(3) 1_655
O4 OH4 O3  0.847(18) 1.551(18) 2.394(2) 174(3) .
C2 H2 O2  0.95 2.61 3.442(2) 146.3 1_565
C2 H2 O3  0.95 2.60 3.302(2) 131.2 1_565

_refine_diff_density_max    0.391
_refine_diff_density_min   -0.318
_refine_diff_density_rms    0.086

_shelxl_version_number 2013-2

_shelx_res_file
;
TITL 227-1 in P2(1)/n,  Zn(H2O) (C7H3NO3(HO)) 'C14 H12 N2 O10 '
CELL 0.71073   9.2883   7.8953  10.3048  90.000  95.070  90.000
ZERR    2.00   0.0017   0.0012   0.0019   0.000   0.005   0.000
```

```
LATT  1
SYMM 0.5-X, 0.5+Y, 0.5-Z
SFAC C  N O  H  ZN
UNIT 28 4 20 24  2
TEMP -80
ACTA
SIZE  0.25 0.25 0.16

OMIT    -5   0   5
OMIT     4   4   2
L.S. 15
BOND $H
HTAB
EQIV $1 -x+1/2, y-1/2, -z+3/2
EQIV $2 x+1, y, z
EQIV $3 x, y+1, z

HTAB O1 O5_$1
HTAB O1 O5_$2
HTAB O4 O3
HTAB C2 O2_$3
HTAB C2 O3_$3
FMAP 2
PLAN 20

WGHT    0.048700    0.465900
FVAR       0.13575
ZN1   5    0.500000    0.500000    0.500000    10.50000    0.01279    0.01647 =
      0.02746    0.00102    0.00827    0.00127
O1    3    0.606776    0.559020    0.692419    11.00000    0.01787    0.02572 =
      0.02671    0.00249    0.00418   -0.00336
DFIX O1 OW1 0.82 0.02
OW1   4    0.623464    0.468712    0.728811    11.00000   -1.50000
DFIX O1 OW2 0.82 0.02
OW2   4    0.677556    0.617732    0.688790    11.00000   -1.50000

O2    3    0.360369    0.338481    0.582379    11.00000    0.01571    0.01603 =
      0.02884    0.00178    0.00706    0.00241
O3    3    0.144199    0.311222    0.649678    11.00000    0.01871    0.01775 =
      0.03570    0.00263    0.01017   -0.00116
O4    3   -0.051212    0.481683    0.712477    11.00000    0.02084    0.02489 =
      0.05072    0.00465    0.01916    0.00290
DFIX O4 OH4 0.82 0.02
OH4   4    0.014314    0.415191    0.691269    11.00000   -1.50000

O5    3   -0.129787    0.740530    0.687795    11.00000    0.01444    0.02785 =
      0.03615   -0.00463    0.00756    0.00188
N1    2    0.334014    0.662088    0.536860    11.00000    0.01329    0.01638 =
      0.02091   -0.00054    0.00435    0.00002
C1    1    0.337174    0.826914    0.511457    11.00000    0.01826    0.01752 =
      0.02670    0.00197    0.00687   -0.00132
AFIX  43
H1    4    0.417707    0.872471    0.472565    11.00000   -1.20000
AFIX   0
C2    1    0.226851    0.933728    0.539951    11.00000    0.02471    0.01585 =
```

```
      0.03018    0.00132    0.00544    0.00177
AFIX  43
H2    4    0.231062    1.051724    0.522640    11.00000   -1.20000
AFIX   0
C3    1    0.110894    0.864170    0.594066    11.00000    0.01926    0.01825 =
      0.02450   -0.00079    0.00339    0.00596
AFIX  43
H3    4    0.033583    0.935402    0.614409    11.00000   -1.20000
AFIX   0
C4    1    0.103906    0.690838    0.619958    11.00000    0.01353    0.01910 =
      0.01618   -0.00094    0.00170    0.00039
C5    1    0.221162    0.591529    0.589985    11.00000    0.01280    0.01658 =
      0.01657   -0.00098    0.00093   -0.00033
C6    1    0.243012    0.399752    0.608840    11.00000    0.01551    0.01645 =
      0.01742   -0.00021    0.00265    0.00040
C7    1   -0.034440    0.635554    0.677287    11.00000    0.01389    0.02443 =
      0.02041   -0.00333    0.00292   -0.00033
REM R1 =  0.0841 for   1713 Fo > 4sig(Fo)  and  0.0865 for all   1817 data
REM    152 parameters refined using      0 restraints

HKLF 4

REM  227-1 in P2(1)/n,  Zn(H2O) (C7H3NO3(HO)) 'C14 H12 N2 O10 '
REM R1 =  0.0298 for    1710 Fo > 4sig(Fo)  and  0.0318 for all    1815 data
REM    133 parameters refined using      3 restraints

END
```